Optical Materials 174 (2026) 117939

Contents lists available at ScienceDirect

Optical Materials

journal homepage: www.elsevier.com/locate/optmat

Effect of the ligand polarizability on the hypersensitive $^5D_0 \rightarrow {}^7F_2$ transition of Eu(III) in nitrate complexes with nitrogen-based ligands

Silvia Ruggieri [a], Albano N. Carneiro Neto [b,*], Carlos V. Santos Jr. [c], Renaldo T. MouraJr [d,e], Marco Bettinelli [a], Fabio Piccinelli [a,**]

[a] Luminescent Materials Laboratory, DB, University of Verona, and INSTM, UdR Verona, Strada Le Grazie 15, Verona, 37134, Italy
[b] Max-Planck-Institut für Kohlenforschung, Kaiser-Wilhelm-Platz 1, Mülheim an der Ruhr, D-45470, Germany
[c] Department of Chemistry, Federal University of Paraiba, João Pessoa, Brazil
[d] Academic Unit of Cabo de Santo Agostinho, Federal Rural University of Pernambuco (UFRPE), Cabo de Santo Agostinho, 54518-430, Brazil
[e] Department of Chemistry, Southern Methodist University, Dallas, TX, 75275-0314, United States

ARTICLE INFO

Keywords:
Eu(III)
Hypersensitive transition
Coordination compounds
Ligand polarizability
Luminescence

ABSTRACT

In this contribution, the *f-f* spectroscopy of two racemic nitrate Eu(III) complexes containing an imine-based (*i.e.* [N,N′-bis(2-pyridylmethylidene)-1,2-(R,R)+(S,S)-cyclohexanediamine]) (**complex 1**) and an amine-based (*i.e.* [N,N′-bis(2-pyridylmethylene)-1,2-(R,R + S,S)-cyclohexanediamine]) (**complexes 2**) ligands has been revisited, in the light of the recent redefinition of the "asymmetry ratio" *R2* [$I(^5D_0 \rightarrow {}^7F_2)$ /$I(^5D_0 \rightarrow {}^7F_1)$] as "hypersensitive ratio", with regard to the luminescence in the visible spectral range of Eu(III) ion, stemming from the $^5D_0$ level. We demonstrate, by means of computational calculations, that *R2* directly connected to the Ω_2 intensity parameter, in turn dominated by a dynamic ligand polarization mechanism (dynamic coupling, DC), is significantly affected by the polarizability of the oxygen and nitrogen ligating atoms, more than by the geometric environment around Eu(III). The larger *R2* value of **complex 1** is ascribable to the lower polarizability of the sp^2 hybridized nitrogens of the iminic ligand involved in the resonance phenomenon together with the heteroaromatic pyridine rings.

1. Introduction

To date, the major uses of Eu(III) ions are in red phosphors and electroluminescent devices [1]. New suggested applications include quantum information systems [2] and remote temperature measurements [3,4]. Whilst Eu(III) 4f-4f emission peak positions do not change significantly, the relative intensities of the bands vary remarkably between different systems [5,6]. Emission transitions from $^5D_0$ to lower ^7F_J (J = 0-6) multiplets are located in the red-to-NIR spectral range.

The emission intensity ratio *R*2, defined as $I(^5D_0 \rightarrow {}^7F_2)/I(^5D_0 \rightarrow {}^7F_1)$, widely defined as the "asymmetry ratio" [7–9], is often associated only with the site symmetry of the Eu(III) ion. However, Thor et al. [10] recently detailed the intrinsic nature of Eu(III) spectral intensity, focusing on the hypersensitive $^5D_0 \rightarrow {}^7F_2$ transition in the frame of the Judd-Ofelt theory [11,12]. They emphasized that the oscillator strength of this transition depends on the Ω_2 parameter, which consists of two contributions: the forced electric dipole (FED, or static coupling) and a dynamic ligand polarization mechanism (dynamic coupling, DC), being the latter predominant for the case of Eu(III) coordination compounds. Consequently, Thor et al. [10] proposed the new term "hypersensitive ratio" instead of "asymmetry ratio" because the $^5D_0 \rightarrow {}^7F_2$ transition not only depends on the symmetry, but also on the polarizabilities of the chemical environment around the Eu(III) ion.

The radiative probability of the $^5D_0 \rightarrow {}^7F_2$ transition (and consequently the value of the hypersensitive ratio *R2*) is quantitatively explained by the dynamic coupling mechanism. Therefore, the most important parameters affecting the $^5D_0 \rightarrow {}^7F_2$ emission intensity (and *R2*

This article is part of a special issue entitled: in honour to Georges Boulon published in Optical Materials.

* Corresponding author.
** Corresponding author.
E-mail addresses: neto@kofo.mpg.de (A.N. Carneiro Neto), fabio.piccinelli@univr.it (F. Piccinelli).

https://doi.org/10.1016/j.optmat.2026.117939
Received 30 November 2025; Received in revised form 24 January 2026; Accepted 2 February 2026
Available online 6 February 2026

values) are the Eu(III) site symmetry, Eu-Ligand distances, ligand polarizability, and configurations that mix with $4f^6$. In other words, the *R2* cannot be attributed solely to site symmetry. Furthermore, the approximation by Mason et al. [13] to Ω_2 is possible due to the minimal participation of the FED mechanism in Eu(III) coordination compounds [14], where the electronic density near the Eu(III) center is soft and highly polarizable.

In this contribution, we revisit the spectroscopic data of two Eu(III) complexes previously investigated by some of us [15]. These complexes are illustrated in Scheme 1 and constituted by the racemic imine ligand [N,N′-bis(2-pyridylmethylidene)-1,2-(R,R)+(S,S)-cyclohexanediamine] (**complex 1**) and the amine ligand [N,N′-bis(2-pyridylmethylene)-1,2-(R,R + S,S)-cyclohexanediamine] (**complexes 2a** and **2b**).

In particular, we have focused our attention on the hypersensitive ratio of the Eu(III) ion in these two complexes differing by the nature of a couple of nitrogen atoms (imine N possessing sp^2 hybridization in **complex 1** and amine N possessing sp^3 hybridization in **complexes 2A** and **2B**). Although the same Eu(III) site symmetry present in these two types of complexes, different *R2* values have been measured. These values have been confirmed by theoretical calculations and the main structural and electronic factors affecting the intensity of the hypersensitive $^5D_0 \rightarrow {}^7F_2$ transition, have been considered and rationalized.

2. Materials and methods

2.1. Synthesis and structural characterization

Complexes **1** and **2** have been synthesized and structurally characterized by Single Crystal X-ray Diffraction (SC-XRD) technique, as reported in Ref. [15].

CCDC 837304 and 837305 contain the supplementary crystallographic data for complexes **1** and **2**. These data can be obtained free of charge from The Cambridge Crystallographic Data Centre via www.ccdc.cam.ac.uk/data_request/cif.

2.2. Photoluminescence

Photoluminescence measurements were carried out as reported in Ref. [15], on powdered samples possessing the same crystal structure discussed in that contribution.

3. Theoretical calculations

All electronic structure calculations were performed using ORCA version 6.1 [16]. We employed the Density Functional Theory (DFT) method with the ωB97X-D3 functional [17,18], which incorporates long-range correction and empirical dispersion correction [19]. The basis set utilized for all atoms except Eu was the split-valence quality def2-TZVP [20]. The MWB28 basis set and effective core potential (ECP) for the Eu atom were applied to account for relativistic effects [21]. To enhance computational efficiency, the def2/J auxiliary basis set [22] was used in conjunction with the Coulomb fitting technique. All calculations were single-point energy evaluations based on the crystallographic geometry of the neutral complexes.

To gain a deeper understanding of how the electronic density on the coordinating atoms affects the hypersensitive ratio, we define the chemical environment's electronic density ρ' associated with a ligating atom (A) and the atoms bonded with it (B). We quantify ρ' using Eq. (1):

$$\rho'(\vec{r}) = 2\sum_{l}^{MOs} n_l \sum_{a\epsilon A}^{N} \sum_{b\epsilon B}^{N} c_a^l \phi_a(\vec{r}) c_b^l \phi_b(\vec{r}) \quad (1)$$

where n_l is the molecular orbital occupation, c_a^l and c_b^l are the coefficients from the linear combination of atomic orbitals expansion for atoms A and B, respectively, and ϕ_a and ϕ_b represent the contracted functions that describe the atomic orbitals. The density is calculated using the ChemBOS (Chemical Bond Overlap Software) [22,23]. In addition to the numerical value, electronic maps that illustrated this density were also generated. The entire process was done for all atoms in the first coordination sphere of the complexes, in order to better understand how the changes in the ligand structure modify the chemical environment of the Eu(III) ion.

The FED contribution to Ω_2 involves the odd-rank crystal field parameters, described by mixed parity states, such as 4*f*-5*d*, 4*f*-5*g*, and continuum states [13]. However, the DC mechanism is often dominant in determining the value of Eu(III)-based compounds [14]. Thus, the Ω_2 (DC) can be easily calculated through the approximation by Mason et al. [13,24]:

$$\Omega_2(DC) \cong \frac{28}{5}\langle 4f|r^2|4f\rangle^2 \sum_{m=0}^{3}(2-\delta_{m,0})\left|\sum_j \frac{\overline{\alpha}_j}{R_j^4}\left(C_m^{(3)}\right)_j\right|^2 \quad (2)$$

In determining the Ω_2 (DC) these parameters are quite significant:

1) $\overline{\alpha}$ is the mean polarizability contribution of each ligand *j* (a parcel of the ligating atom isotropic polarizability which interacts with the lanthanide),
2) *R* is the metal-ligand bond distance, and
3) $C_m^{(3)}$ is a third-rank spherical tensor.

The latter is dependent on the coordination symmetry around Eu (III). For didactic purposes, the demonstration of equation (2) is detailed

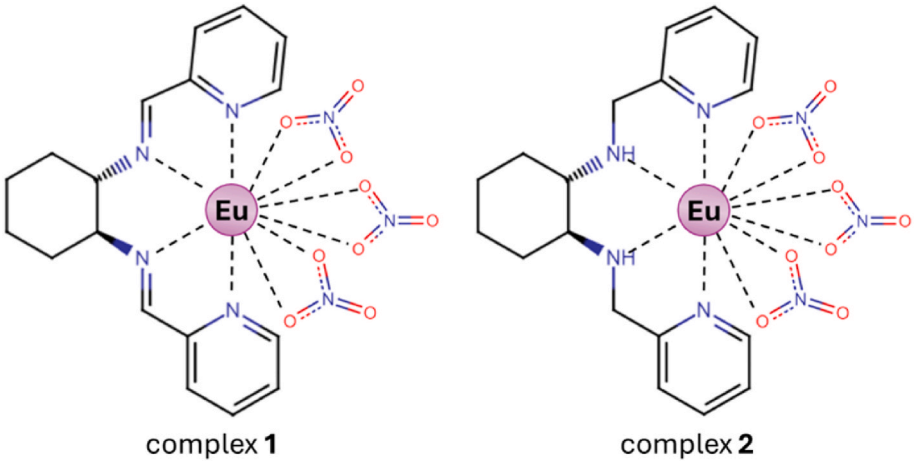

complex **1** complex **2**

Scheme 1. Molecular structures of the complexes under consideration in this work. Only the (*S,S*) enantiomer of the racemic mixture is depicted.

in the Supporting Information.

With the values of $\Omega_2(DC)$, the *R2* parameter can be estimated through [10]:

$$R2 \cong \Omega_2(DC) \cdot C \cdot \left(\frac{n^2+2}{3n}\right)^2 \quad (3)$$

where $C = 6.6 \times 10^2$ cm^{-2} is a constant and n is the index of refraction of the medium, considered n = 1.5 in this work, which is a common acceptable value for lanthanide-based coordination compounds in the solid-state [10,25].

4. Results and discussion

4.1. Structural characterization of complexes *1* and *2*

As already reported in our previous contribution [15] the molecular structure of the complex **1** and **2** has been characterized by single X-ray diffraction on single crystals. The reader is referred to this contribution, for the full and detailed description of the structures and the crystal packings. Here, we report the main structural features of these molecules (Fig. 1). Both complexes crystallize as racemates in centric space groups ($P2_1/c$ for complex **1** and *Pbca* for complex **2**). One solvent molecule (acetonitrile), omitted here for sake of clarity, is present in the crystals of complex **1**.

The Eu(III) ion exhibits a 10-fold coordination, characterized by four nitrogen atoms from the tetradentate ligand and six oxygen atoms from three nitrate molecules. In the structure of complex **2**, we observed the presence of two conformational isomers (**2A** and **2B**), which differ slightly in the position of the nitrate anions and the hydrogen atoms bound to the ligand's nitrogens, N9 and N10, in the position labeled as "external" (Fig. 1). The relative occupancy is 0.66 for conformer **2A** and 0.34 for conformer **2B**.

The observed coordination polyhedra are distorted sphenocoronas in the case of complex **1** and complex **2** (conformer **A**), and a bicapped square antiprism for conformer **B** of complex **2**. The bond distances involving the Eu(III) ion in the two complexes are reported in Table S1.

From a close inspection of Table S1, we can conclude that in the two isomeric conformers of the amine-based complex **2**, the Eu–N bond distances are similar, regardless of the different hybridization of the nitrogen atoms in the ligand [sp^3 for N (9) and N (10), sp^2 for N (7) and N (8)]. On the contrary, as already discussed previously [15], nitrogen atoms exhibiting the same hybridization in the imine-based complex **1**

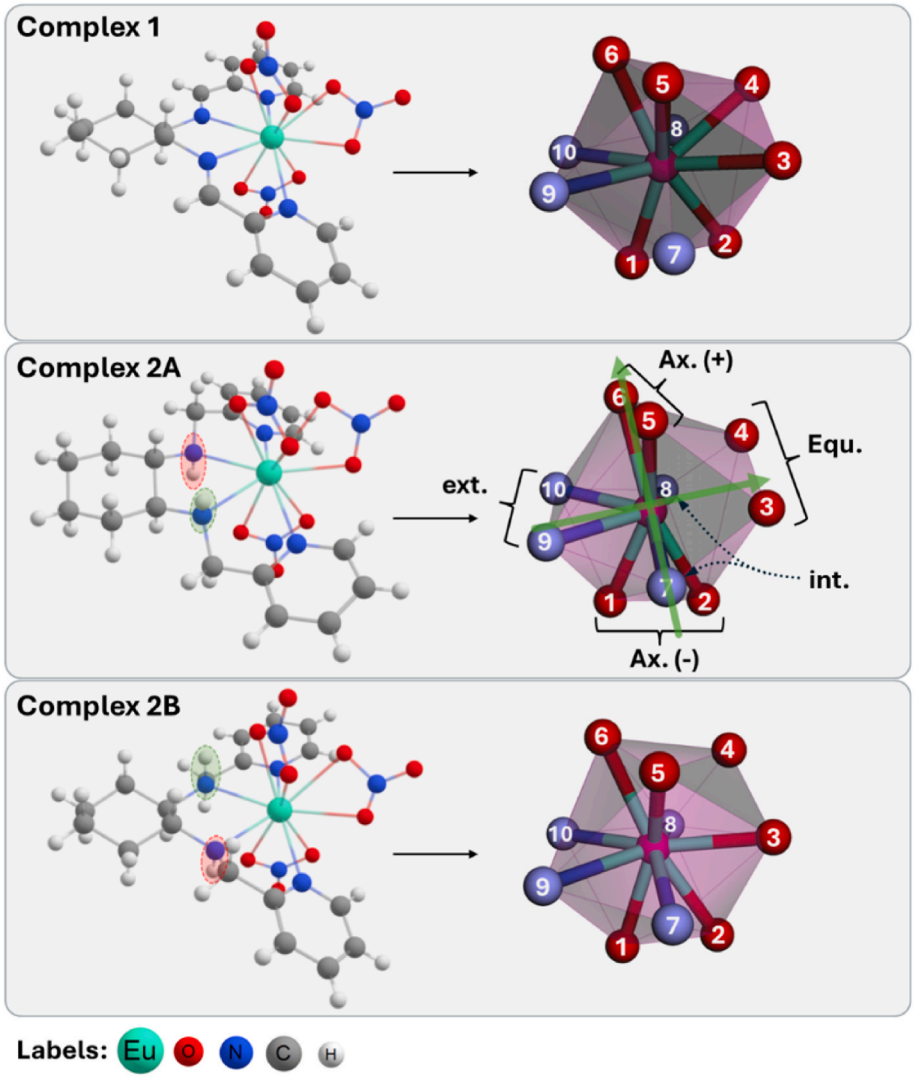

Fig. 1. Molecular structures of **Complexes 1, 2a and 2b**. The coordination polyhedra are also shown and it can be noticed that there are no drastic differences between them. The indications shown in **2a** are labels to guide the calculations through different ligand groups. The labels ***Equ.***, ***Ax. (−)***, ***Ax. (+)*** indicate the NO_3^- groups that are in the equatorial, positive and negative parts of the imaginary axes highlighted in green. The labels ***ext.*** and ***int.*** define the external and internal nitrogen atoms of the main ligand. (For interpretation of the references to colour in this figure legend, the reader is referred to the Web version of this article.)

[sp^2 for all the N atoms] showed different Eu–N bond distances. In particular, the bonds involving pyridine nitrogen are longer (on average 2.63 Å) than the ones involving imine nitrogen (2.55 Å). These features are attributable to crystal packing effects. In addition, whilst in the complex **1** each nitrate is bound to the metal ion with two almost equivalent bond contacts (*i.e.* as a bidentate ligands), in the dominant conformational isomer **2A**, the coordination of the nitrates is more asymmetric, in particular for one of these (Eu–O (4) 2.644 (4) Å and Eu–O (3) 2.506 (8) Å).

In all cases, the Eu(III) point symmetry is C_1. The values of the root mean square deviation (RMSD) of Cartesian coordinates (x,y,z) between the coordination polyhedra (considering only the atoms in the coordination polyhedra) are shown in Table S2. For instance, the coordination polyhedron of complex **1** and complex **2B** have a lower RMSD value (0.219842 Å) compared to the polyhedra of conformers **2A** and **2B** (RMSD = 0.365234 Å). This indicates that despite the different sp^2 hybridization in **1** and the sp^3 hybridization in **2A** and **2B**, all complexes are structurally similar. Thus, this reinforces that the symmetry alone cannot account for the major differences observed in the intensity of the hypersensitive $^5D_0 \rightarrow {}^7F_2$ emission.

4.2. Spectroscopic characterization of complexes *1* and *2*

The emission spectra of the complexes **1** and **2**, upon direct excitation at 465 nm in the $^5D_2$ level of Eu(III), are reported in Fig. 2. These spectra were normalized according to the $^5D_0 \rightarrow {}^7F_1$ transition to better represent the hypersensitive ratio (*R2*).

All the expected emission peaks, stemming from $^5D_0$ level of Eu(III) ($^5D_0 \rightarrow {}^7F_J$; J = 0-4) are detected. It is worth noting that the Stark components of each transition are similar between these two complexes, indicating that only minor structural differences exist between them, as confirmed previously by the RMSD values.

The values of the experimental hypersensitive ratio (*R2*) were estimated using the JOYSpectra web platform [26,27], specifically through the spectrum analysis tool, accessible via http://www.joyspectra.com.br. The calculated values are 6.77 for complex **1** and 4.64 for complex **2**. It is important to note that it is not possible to discriminate the single spectral contribution of the isomers **2A** and **2B** to the total emission spectrum. Therefore, the *R2* value calculated for complex **2**, should be regarded as the average contribution weighted by the occupation factors of each isomer. We also already discussed the presence of two components for the $^5D_0 \rightarrow {}^7F_0$ transition in the complex **2** (inset of Fig. 2, blue line), one for each conformer, in agreement with the Eu(III) axial point symmetry observed in both isomers (C_1 point symmetry) [15]. As expected, as proof of Eu(III) point symmetry lacking the inversion center element, the hypersensitive $^5D_0 \rightarrow {}^7F_2$ transition dominates the emission spectra of both complexes. Interestingly, despite the identical Eu(III) point symmetry (C_1), the values of the hypersensitive ratio are significantly different for the two complexes. In agreement with the conclusion drawn by Thor et al. [10], *R2* value calculated from the Eu(III) emission spectra, cannot only be considered as a marker of Eu(III) site/point symmetry.

4.3. Relationship between the spectroscopic and structural/electronic properties of the complexes

The calculations regarding the atomic polarizabilities serve as a guide to check how the Eu(III) ion is affected by the dynamic coupling mechanism.

The value of the polarizabilities (α in units of Å^3) and electronic density (ρ' in units of e/a_0^3) are presented in Table S3. It is noticeable that the oxygen atoms (all belonging to NO_3^- groups) have a similar average density of 8.31 ± 0.04 e/a_0^3, while the nitrogen (N) atoms of the main ligand present a lower average density of 7.18 ± 0.04 e/a_0^3.

The calculated isotropic polarizabilities follow the same trend as the densities, with O ligands presenting values around 2.4 ± 0.8 Å^3 and the N atoms of the main ligand presenting 1.1 ± 0.6 Å^3. However, these raw polarizability values cannot be used directly in Equation (2) because the Eu(III) ion does not interact with the entire density of the ligating atom. Consequently, we established a unique set of mean polarizabilities $\bar{\alpha}$ based on the density trends (Fig. 3, represented in symbols: squares, triangles and circles). We attributed a value of 2.2 Å^3 for each O atom in the NO_3^- ligands, regardless of the compound (**1**, **2A**, or **2B**).

The $\bar{\alpha}$ value for the N atoms follows the same trend as ρ' (Fig. 3 and Table S4), being generally lower than the O atoms. In complex **1**, electronic resonance effects likely lead to a more displaced electronic density through the ligand, resulting in the N atom in the "external" position (N9 and N10) having a higher electronic density than the N atom in the "internal" position (N7 and N8) compared to compounds **2A** and **2B** (Fig. 3c). This is expected to reflect a more significant polarizable difference between the internal and external N atoms in complex **1**.

In fact, complex **1** presented a higher Ω_2 and *R2* value due to the lower polarizability of the N7 and N8 atoms ($\bar{\alpha} = 0.2$ Å^3; blue circles in Fig. 3b) compared to the values of **2A** and **2B** ($\bar{\alpha} = 1.2$ Å^3; Fig. 3b). This

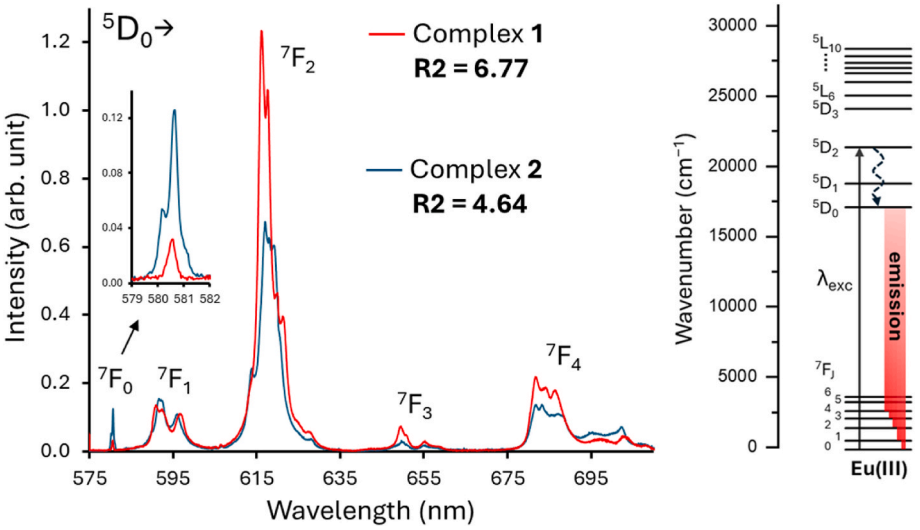

Fig. 2. Emission spectra of complexes **1** and **2**, normalized to the area of the $^5D_0 \rightarrow {}^7F_1$ peak (left panel), upon excitation at $\lambda_{exc} = 465$ nm ($^7F_0 \rightarrow {}^5D_2$), as represented in the right panel. The values of the hypersensitive ratio *R2* are also presented. The inset shows the $^5D_0 \rightarrow {}^7F_0$ emissions, which indicate that complex **2** has two distinct peaks attributed to its two conformers.

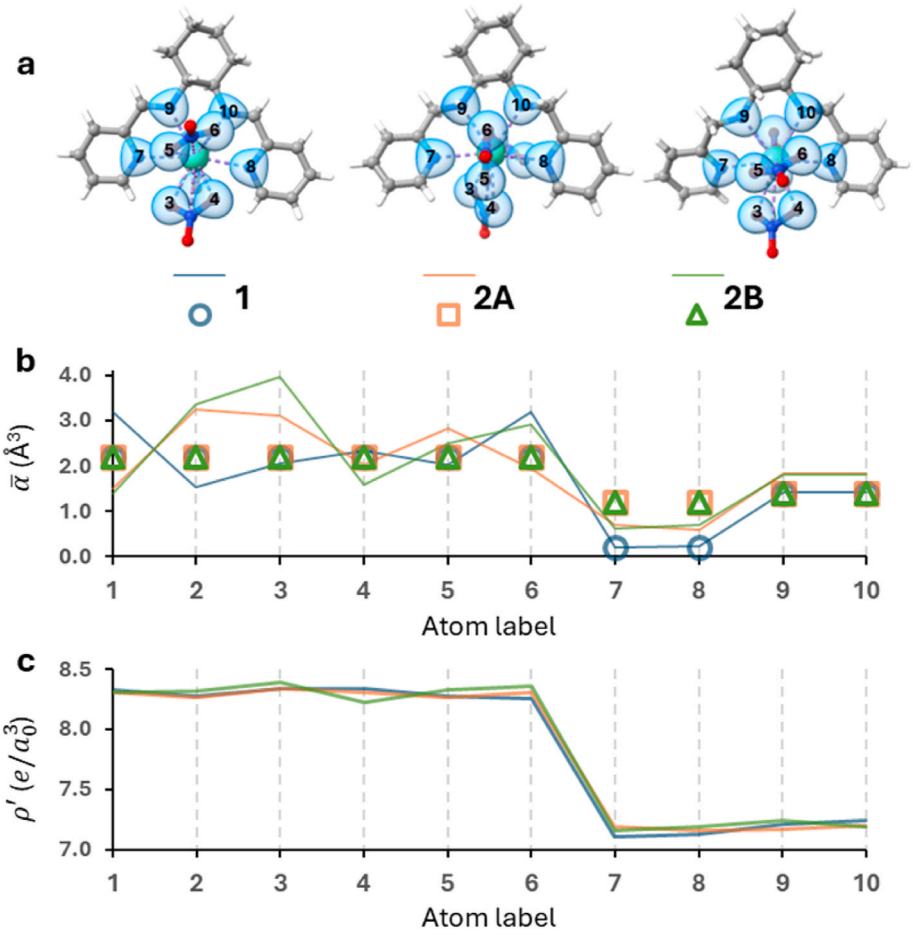

Fig. 3. Electronic properties of the coordinating atoms for complexes **1**, **2A**, and **2B**. a) Electronic density maps obtained using 8ChemBOS [23,28] software and plotted in ChimeraX [29] using isovalues of 0.07 e/a_0^3. b) Calculated (α, lines) and applied ($\overline{\alpha}$, symbols) values of polarizabilities. c) Values of calculated densities (ρ').

low value of $\overline{\alpha}$ in N7 and N8 for complex **1** breaks the symmetry by polarizability rather than by geometric aspects. In other words, such discrepancy of $\overline{\alpha}$ values among nitrogen atoms makes the deletion of terms related to the mean polarizability ($\overline{\alpha}$) in the last summation of equation (2), less effective.

With the values of $\overline{\alpha}$ alongside with the angles of the spherical coordinates centered at the Eu(III) site (Table S4, bond distances are in Table S1), the obtained values of Ω_2 and *R2* for each compound are presented in Table 1. The experimental values were obtained by uploading the emission spectra of the complexes to the JOYSpectra web platform (http://www.joyspectra.com.br) [26,27] and the pictures of this analysis is also in the Supporting Information.

Due to the very similar structure of isomers **2A** and **2B**, they are expected to have the same set of mean polarizabilities $\overline{\alpha}$ (Table S4 and Fig. 3). The differences in their Ω_2 values are thus primarily attributable to slight changes in their structures, allowing two theoretical Ω_2 values to be calculated for the isomers of complex **2**. The final theoretical Ω_2 value for complex **2** is then a weighted average based on the occupation numbers: 0.66 for **2A** and 0.34 for **2B**. Thus, taking the average value of the theoretical data for Ω_2 and *R2*, it is obtained:

$$\Omega_2\ (\text{av.}) = \left(0.66 \times 9.41 \times 10^{-20}\ \text{cm}^2\right) + \left(0.34 \times 5.26 \times 10^{-20}\ \text{cm}^2\right) = 8.00 \times 10^{-20}\ \text{cm}^2,$$

This result is in agreement with the experimentally obtained value of 7.84×10^{-20} cm^2.

Table 1
Experimental e theoretical values of Ω_2 and *R2* for the complexes **1**, **2A** and **2B**.

	Experimental		Theoretical	
	Ω_2 ($\times 10^{-20}$ cm^2)	*R2*	Ω_2 ($\times 10^{-20}$ cm^2)	*R2*
1	11.39	6.77	11.18	6.58
2A	7.84	4.65	9.41	5.54
2B	7.84	4.65	5.26	3.10

5. Conclusions

In this contribution, we demonstrate by a combined experimental and theoretical investigation that although the two complexes **1** and **2** exhibit the same Eu(III) point symmetry (C_1), their "hypersensitive ratio" values *R2* are significantly different. In particular, in the case of the imine-based complex **1**, it is around 1.5 times larger than for the amine-based one (complex **2**). The lower polarizability of the sp^2 nitrogen atoms of the imine functional groups is mainly responsible for this behavior. The type of hybridization of the two non-pyridinic nitrogen atoms (sp^2 in complex **1** and sp^3 in complex **2**) determines whether these atoms are involved in the conjugation with the electronic π-system of the pyridine rings. When conjugation occurs (*i.e.* for sp^2 nitrogen atoms), a lower polarizability of the pyridine nitrogens is observed, breaking the symmetry of the distribution of the polarizabilities of the N donor atoms around the metal ion, and this promotes a higher R2 value. Our contribution further demonstrates that the "asymmetry ratio" of the Eu(III) luminescence cannot only be considered as a marker of Eu(III) site/point symmetry, as some people believe, but it is also strongly dependent on the polarizability of the ligand

donating atoms around the metal ion. To the best of our knowledge, this is the first example in which two almost isostructural Eu(III) nitrate complexes of tetraaza (N4) ligands, exhibit such a marked difference in the "hypersensitive ratio" values of the metal ion.

CRediT authorship contribution statement

Silvia Ruggieri: Formal analysis. **Albano N. Carneiro Neto:** Conceptualization, Writing – original draft. **Carlos V. Santos:** Validation. **Renaldo T. MouraJr:** Data curation, Supervision. **Marco Bettinelli:** Supervision, Validation. **Fabio Piccinelli:** Conceptualization, Writing – original draft, Writing – review & editing.

Declaration of competing interest

The authors declare that they have no known competing financial interests or personal relationships that could have appeared to influence the work reported in this paper.

Acknowledgments

The Brazilian Agencies FACEPE, CAPES, CNPq, FINEP, and INCT-LumiNanoTec are acknowledged for providing partial financial support under grant numbers: 408501/2024-3. APQ-1636-1.06/24, and APQ-1056-1.06/22. RTMJr thanks the Brazilian National Council for Scientific and Technological Development - CNPq, Grant numbers 406483/2023-0, 310988/2023-3, and 404742/2024-6. The authors would like to dedicate this paper to the memory of Georges Boulon.

Appendix A. Supplementary data

Supplementary data to this article can be found online at https://doi.org/10.1016/j.optmat.2026.117939.

Data availability

Data will be made available on request.

References

[1] K. Nehra, A. Dalal, A. Hooda, S. Bhagwan, R.K. Saini, B. Mari, S. Kumar, D. Singh, Lanthanides β-diketonate complexes as energy-efficient emissive materials: a review, J. Mol. Struct. 1249 (2022) 131531, https://doi.org/10.1016/j.molstruc.2021.131531.

[2] Z.W. Riedel, D.R. Pearson, M.H. Karigerasi, J.A.N.T. Soares, E.A. Goldschmidt, D. P. Shoemaker, Synthesis of $Eu(HCOO)_3$ and $Eu(HCOO)_3{\bullet}(HCONH_2)_2$ crystals and observation of their $^5D_0 \rightarrow {}^7F_0$ transition for quantum information systems, J. Lumin. 249 (2022) 119006, https://doi.org/10.1016/j.jlumin.2022.119006.

[3] L. Blois, A.N. Carneiro Neto, O.L. Malta, H.F. Brito, A theoretical framework for optical thermometry based on excited-state absorption and lifetimes of Eu^{3+} compounds, J. Lumin. 249 (2022) 119039, https://doi.org/10.1016/j.jlumin.2022.119039.

[4] C.D.S. Brites, R. Marin, M. Suta, A.N. Carneiro Neto, E. Ximendes, D. Jaque, L. D. Carlos, Spotlight on luminescence thermometry: basics, challenges, and cutting-edge applications, Adv. Mater. 35 (2023) 2302749, https://doi.org/10.1002/adma.202302749.

[5] M. Bettinelli, A. Speghini, F. Piccinelli, A.N.C. Neto, O.L. Malta, Spectroscopy of Eu^{3+} in $Ca_3Sc_2Si_3O_{12}$, J. Lumin. 131 (2011) 1026, https://doi.org/10.1016/j.jlumin.2011.01.016.

[6] F. Piccinelli, I. Carrasco, C.-G. Ma, A.M. Srivastava, M. Bettinelli, Disorder-induced breaking of the local inversion symmetry in rhombohedral pyrochlores $M_2La_3Sb_3O_{14}$ (M = Mg or Ca): a structural and spectroscopic investigation, Inorg. Chem. 57 (2018) 9241, https://doi.org/10.1021/acs.inorgchem.8b01261.

[7] M. Gaft, G. Panczer, R. Reisfeld, I. Shinno, B. Champagnon, G. Boulon, Laser-induced Eu^{3+} luminescence in zircon $ZrSiO_4$, J. Lumin. 87–89 (2000) 1032–1035, https://doi.org/10.1016/S0022-2313(99)00530-X.

[8] E.W.J.L. Oomen, A.M.A. van Dongen, Europium (III) in oxide glasses: dependence of the emission spectrum upon glass composition, J. Non-Cryst. Solids 111 (1989) 205–213, https://doi.org/10.1016/0022-3093(89)90282-2.

[9] R. Reisfeld, E. Zigansky, M. Gaft, Europium probe for estimation of site symmetry in glass films, glasses and crystals, Mol. Phys. 102 (2004) 1319–1330, https://doi.org/10.1080/00268970410001728609.

[10] W. Thor, A.N. Carneiro Neto, R.T. Moura, K.-L. Wong, P.A. Tanner, Europium(III) coordination chemistry: structure, spectra and hypersensitivity, Coord. Chem. Rev. 517 (2024) 215927, https://doi.org/10.1016/j.ccr.2024.215927.

[11] B.R. Judd, Optical absorption intensities of rare-earth ions, Phys. Rev. 127 (1962) 750–761, https://doi.org/10.1103/PhysRev.127.750.

[12] G.S. Ofelt, Intensities of crystal spectra of rare-earth ions, J. Chem. Phys. 37 (1962) 511–520, https://doi.org/10.1063/1.1701366.

[13] S.F. Mason, R.D. Peacock, B. Stewart, Ligand-polarization contributions to the intensity of hypersensitive trivalent lanthanide transitions, Mol. Phys. 30 (1975) 1829–1841, https://doi.org/10.1080/00268977500103321.

[14] R.T. Moura Jr., A.N. Carneiro Neto, R.L. Longo, O.L. Malta, On the calculation and interpretation of covalency in the intensity parameters of 4f-4f transitions in Eu^{3+} complexes based on the chemical bond overlap polarizability, J. Lumin. 170 (2016) 420–430, https://doi.org/10.1016/j.jlumin.2015.08.016.

[15] F. Piccinelli, A. Speghini, M. Monari, M. Bettinelli, New chiral pyridine-based Eu (III) complexes: study of the relationship between the nature of the ligands and the $^5D_0$ luminescence spectra, Inorg. Chim. Acta. 385 (2012) 65–72, https://doi.org/10.1016/j.ica.2011.12.042.

[16] F. Neese, Software update: the *ORCA* program system—version 6.0, WIREs Computational Molecular Science 15 (2025), https://doi.org/10.1002/wcms.70019.

[17] J.-D. Chai, M. Head-Gordon, Long-range corrected hybrid density functionals with damped atom–atom dispersion corrections, Phys. Chem. Chem. Phys. 10 (2008) 6615, https://doi.org/10.1039/b810189b.

[18] Y.S. Lin, G. De Li, S.P. Mao, J. Da Chai, Long-range corrected hybrid density functionals with improved dispersion corrections, J. Chem. Theor. Comput. 9 (2013) 263–272, https://doi.org/10.1021/ct300715s.

[19] S. Grimme, J. Antony, S. Ehrlich, H. Krieg, A consistent and accurate ab initio parametrization of density functional dispersion correction (DFT-D) for the 94 elements H-Pu, J. Chem. Phys. 132 (2010) 154104, https://doi.org/10.1063/1.3382344.

[20] F. Weigend, R. Ahlrichs, Balanced basis sets of split valence, triple zeta valence and quadruple zeta valence quality for H to Rn: design and assessment of accuracy, Phys. Chem. Chem. Phys. 7 (2005) 3297, https://doi.org/10.1039/b508541a.

[21] M. Dolg, H. Stoll, H. Preuss, Energy-adjusted ab initio pseudopotentials for the rare earth elements, J. Chem. Phys. 90 (1989) 1730–1734, https://doi.org/10.1063/1.456066.

[22] F. Weigend, Accurate Coulomb-fitting basis sets for H to Rn, Phys. Chem. Chem. Phys. 8 (2006) 1057, https://doi.org/10.1039/b515623h.

[23] C.V. Santos-Jr, E.M. Lima, R.T. Moura Jr., Numerical integration of overlap electron densities: parallelization strategies for a good load balancing using OpenMP, Comput. Theor. Chem. 1206 (2021) 113457, https://doi.org/10.1016/j.comptc.2021.113457.

[24] R.D. Peacock, The charge-transfer contribution to the intensity of hypersensitive trivalent lanthanide transitions, Mol. Phys. 33 (1977) 1239–1246, https://doi.org/10.1080/00268977700101051.

[25] J.-C.G. Bünzli, S. V Eliseeva, Basics of lanthanide photophysics, in: P. Hänninen, H. Härmä (Eds.), Lanthanide Luminescence: Photophysical, Analytical and Biological Aspects, 7, Springer, Berlin, Heidelberg, 2010, pp. 1–45, https://doi.org/10.1007/4243_2010_3.

[26] Albano N. Carneiro Neto, Eduardo C. Aguiar, Carlos V. Santos-Jr, Ewerton Matias de Lima, Lucca Blois, Oscar L. Malta, Ricardo L. Longo, Elfi Kraka, Renaldo T. Moura JR., The JOYSpectra web platform. http://www.joyspectra.com.br, 2025 (accessed November 6, 2025).

[27] R.T. Moura Jr., A.N. Carneiro Neto, E.C. Aguiar, C.V. Santos-Jr, E.M. de Lima, W. M. Faustino, E.E.S. Teotonio, H.F. Brito, M.C.F.C. Felinto, R.A.S. Ferreira, L. D. Carlos, R.L. Longo, O.L. Malta, JOYSpectra: a web platform for luminescence of lanthanides, Opt. Mater. X 11 (2021) 100080, https://doi.org/10.1016/j.omx.2021.100080.

[28] R.T. Moura, A.N. Carneiro Neto, O.L. Malta, R.L. Longo, Overlap properties of chemical bonds in generic systems including unusual bonding situations, J. Mol. Model. 26 (2020), https://doi.org/10.1007/s00894-020-04535-w.

[29] E.F. Pettersen, T.D. Goddard, C.C. Huang, E.C. Meng, G.S. Couch, T.I. Croll, J. H. Morris, T.E. Ferrin, UCSF ChimeraX: structure visualization for researchers, educators, and developers, Protein Sci. 30 (2021) 70–82, https://doi.org/10.1002/pro.3943.